Astron. Astrophys. 345, 172–180 (1999)

ASTRONOMY
AND
ASTROPHYSICS

Non-radial pulsations in the O stars ξ Persei and λ Cephei

J.A. de Jong[1], **H.F. Henrichs**[1], **C. Schrijvers**[1], **D.R. Gies**[2], **J.H. Telting**[3], **L. Kaper**[1], **and G.A.A. Zwarthoed**[1]

[1] Astronomical Institute 'Anton Pannekoek', University of Amsterdam, Kruislaan 403, 1098SJ Amsterdam, The Netherlands (jdj; huib; coen; lexk@astro.uva.nl)
[2] CHARA, Georgia State University, Atlanta, GA 30303, USA (gies@chara.gsu.edu)
[3] Isaac Newton Group of Telescopes, ASTRON/NFRA, Apartado 321, E-38780 Santa Cruz de la Palma, Spain (jht@ing.iac.es)

Received 27 August 1998 / Accepted 8 February 1999

Abstract. A new time-series analysis of profile changes in the photospheric He I λ4713 spectral line from data taken during 5 days in 1989 at the Calar Alto and Kitt Peak observatories has provided evidence for the presence of a non-radial prograde p-mode in the O 7.5 giant ξ Per (ℓ = 3, P = 3.5) and probably two such modes in the O6 supergiant λ Cep (ℓ = 3, P = 12.3 h and ℓ = 5, P = 6.6 h). The corotating pulsation periods are in both cases much shorter than the estimated stellar rotation period. Modeling the observed amplitude of the line-profile changes (assuming $|m| = \ell$) yields a velocity amplitude of approximately 5 km s^{-1} of the pulsation in ξ Per and 6 km s^{-1} in λ Cep.

Any such a pulsation by itself is unlikely to be the cause of the well-known cyclical wind variability in these stars because the pulsation period is too short, but the cumulative action of multiple modes could cause such an effect. Weak magnetic fields anchored at the surface remain the strongest candidate for the origin of wind variability.

Key words: stars: early-type – stars: individual: ξ Per – stars: individual: λ Cep – stars: mass-loss – stars: winds, outflows

1. Introduction

Pulsating stars are found in nearly every part of the HR diagram. Among O stars, however, only very few pulsators are known. Fullerton et al. (1996) listed 3 confirmed and 6 suspected pulsating O stars and noticed that all these massive stars are located in the instability strip predicted by Kiriakidis et al. (1993). Besides its asteroseismological potential, the search for non-radial pulsations (NRP) in early-type stars is largely motivated by the unknown origin of the widely observed cyclic variability in their winds, notably in the absorption parts of the ultraviolet P Cygni profiles. Most prominent are the migrating discrete absorption components (DACs) with a recurrence time scale that can be interpreted as (an integer fraction of) the stellar rotation period. The cause of the cyclical wind variability is an unsolved issue. It is not known whether the variability is strictly periodic. For example, a comparison of four different datasets obtained in subsequent years of the O7.5III star ξ Persei (Kaper et al. 1999) shows that the dominant period remains 2 (or 4) days, but detailed changes in the variability pattern occur from year to year.

The wind structures can be traced in radial velocity back down to the $v\sin i$ value of the star (see for ξ Per Henrichs et al. 1994, Kaper et al. 1996). This argues in favor of a model with corotating wind structures similar to the Corotating Interaction Regions in the solar wind (CIRs, in the context of hot-star winds first proposed by Mullan 1984). The CIR model invokes fast and slow wind streams that originate at different locations at the stellar surface. Due to the rotation of the star, the wind streams are curved, so that fast wind material catches up with slow material in front forming a shock at the interaction region. The shock pattern in the wind is determined by the boundary conditions at the base of the wind and corotates with the star. In the radiative hydrodynamical computations by Cranmer & Owocki (1996) these spiral-like regions indeed emerge, giving rise to accelerating DACs in wind lines, very similar to what is observed. The key point is, however, that the physical origin of the fast and slow streams is not specified in the calculation: either magnetic fields or non-radial pulsations could equally provide the required differentiation of the emerging wind. In the first case the number of wind structures is determined by the number of magnetic footpoints and the modulation comes directly from the stellar rotation, whereas in the case of a single NRP mode the value of the azimuthal number m determines the azimuthal distribution of the wind structures and the modulation is caused by the traveling speed of the pulsation superposed on the stellar rotation in the observers frame. A third case could also be considered, in which coadding amplitudes of multiple modes may give rise to wind perturbations with a periodic nature depending on the specific modes.

The timescales of pulsation, rotation and wind flow are all on the order of one day, which makes it particularly difficult to disentangle these effects, and which forces a ground-based multi-site approach, preferably simultaneously with UV spectroscopy from space. A different approach has been followed by Howarth et al. (1998), who were able to recover pulsation periods of HD 64760 B0.5Ib and HD 93521 O9.5V derived from UV data by applying cross-correlation techniques. Their

Send offprint requests to: J.A. de Jong

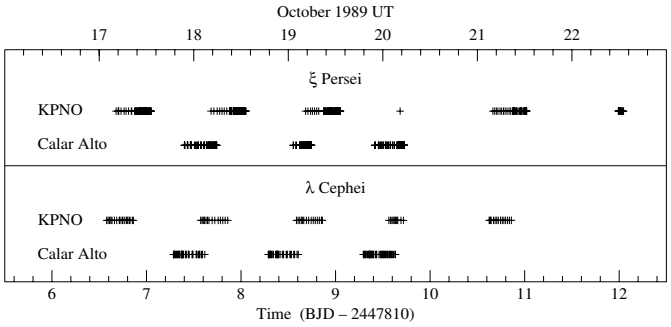

Fig. 1. Schematic time line of the optical spectroscopic observations of the campaign used for the current analysis. In total 324 spectra were selected for ξ Per and 169 for λ Cep

paper is concerned with the same problem as addressed here. In our study we decided to concentrate on the O stars ξ Persei O7.5III(n)((f)) and λ Cephei O6I(n)fp because of their brightness, conveniently close relative location in the sky, excellent record of their UV resonance line behavior, and suitable recurrence period of DACs (1–2 days). The strategy was to probe simultaneously the outer part of the stellar wind (using UV resonance lines), the inner part of the wind (using N IV λ1718 and Hα) and the stellar photosphere (using optical lines). Lines formed deep in the photosphere are used to study pulsation behavior by means of Doppler imaging techniques.

This paper reports the results of a new analysis of the behavior of such a photospheric line He I λ4713 of such a campaign in 1989 during 5 days. Whereas previous analyses of this dataset did not yield convincing results, the advent of new methods of line-profile analysis allowed us to detect the pulsation modes described below.

2. Observations and data reduction

A multi-site campaign was held from 17 to 22 October 1989, including UV spectroscopy with the IUE satellite, optical spectroscopy at the Kitt Peak and Calar Alto observatories, B polarimetry at McDonald Observatory and UBV photometry at the Wendelstein observatory. The IUE spectra are described and analyzed by Kaper et al. (1996, 1999). Here we restrict ourselves to the data that lead to the pulsation analysis.

The experimental setup was chosen in accordance with the $v\sin i$ values of the stars. With 200 km s^{-1} for ξ Per and 214 km s^{-1} for λ Cep (Conti & Ebbets 1977) a resolution of 15 km s^{-1} would give about 25 effective points in the line profile, sufficient to assure that modes up to $\ell \simeq 20$ would be detectable. We concentrated on the weak and therefore deep-seated photospheric He I absorption line at 4713 Å.

The Calar Alto 2.2m telescope (observers GZ and HH) was used with the 90 cm f/3 camera in Coudé focus with grating #1 (632 lines mm^{-1}) in second order centered at 4667 Å, giving a dispersion of 8.6 Å mm^{-1}. We used a RCA CCD chip (#11) with 1024×640 pixels of 15 μm size yielding a coverage of 130 Å with a 2 pixel resolution of 0.26 Å. At this setting the CCD has a quantum efficiency of 68%, which gave 6.7 electrons per count with the gain set at 30. The slitwidth was 1.5 arcsec, equal to the average seeing. At Kitt Peak (observer DG) the 0.9-m Coudé feed was used with camera #5, long collimator with grating A (632 lines mm^{-1}) in second order with a 4–96 filter to block the first order light, yielding a dispersion of 7.1 Å mm^{-1} on the Texas Instruments CCD (TI3) with 800×600 pixels of 15 μm size. This yielded a coverage of 85 Å with a projected slitwidth of 21.3 μ FWHM. The CCD chip has a quantum efficiency of 70%, giving 4.12 electrons per count with the used gain. The slitwidth was fixed at the average seeing of 1.5 arcsec. Typical exposure times were 2 to 3 minutes for ξ Per and 7 to 10 minutes for λ Cep at Calar Alto, and about 1.5 times longer at Kitt Peak. The number of spectra used in the analysis was 324 for ξ Per (154 from Calar Alto and 170 from Kitt Peak), and 169 for λ Cep (109 from Calar Alto and 60 from Kitt Peak). Fig. 1 depicts the time line of the optical spectroscopic observations for both stars.

Flatfielding, bias subtraction and wavelength calibration with Th–Ar lamps were done in the usual manner. The spectra were normalized by using a linear fit through wavelength segments carefully selected to contain no traces of spectral lines. We used [4695.2, 4700.4] and [4720.1, 4723.4]Å for both stars. We also attempted higher-order polynomials, but this did not change the results of the frequency analysis. All spectra were finally smoothed and reduced on a uniform velocity grid of 15 km s^{-1}. Spectra taken at the same epoch at the two observatories showed excellent agreement within the errors given the signal to noise ratio (S/N) which was on average about 800 (Calar Alto) and 500 (Kitt Peak) for ξ Per and 500 (Calar Alto) and 300 (Kitt Peak) for λ Cep, respectively. This agreement was reached after some small night-to-night and observatory-to-observatory wavelength corrections. These were only needed for Calar Alto spectra, because of some technical problems at the telescope that occurred at several nights, which made apparently small changes to the wavelength setting.

Throughout this paper, the reference wavelength for conversion to the stellar restframe has been corrected with 60 and -75 km s^{-1} for the runaway stars ξ Per and λ Cep, respectively (Gies 1987).

Average spectra are shown in the top panels of Figs. 2 and 3. Sample quotient dynamic spectra of ξ Per and λ Cep are in these figures compared with the inverse Fourier transform (after removal of noise) and with folded data using the pulsation frequencies reported in this paper.

3. Period analysis

We performed a standard CLEAN analysis (Roberts et al. 1987, Gies & Kullavanijaya 1988) of the He I λ4713 Å line. The resulting power spectra are shown as grey-scale representations in Figs. 4 and 6. There is considerable power near periods around 1 day and longer, which for both stars we can mostly attribute to wind contaminations, rather than windowing aliases. These low-frequency signals may also partly reflect unaccounted systematic differences between observatories and slight differences in processing of flat fields, normalization, etc. between nights, in

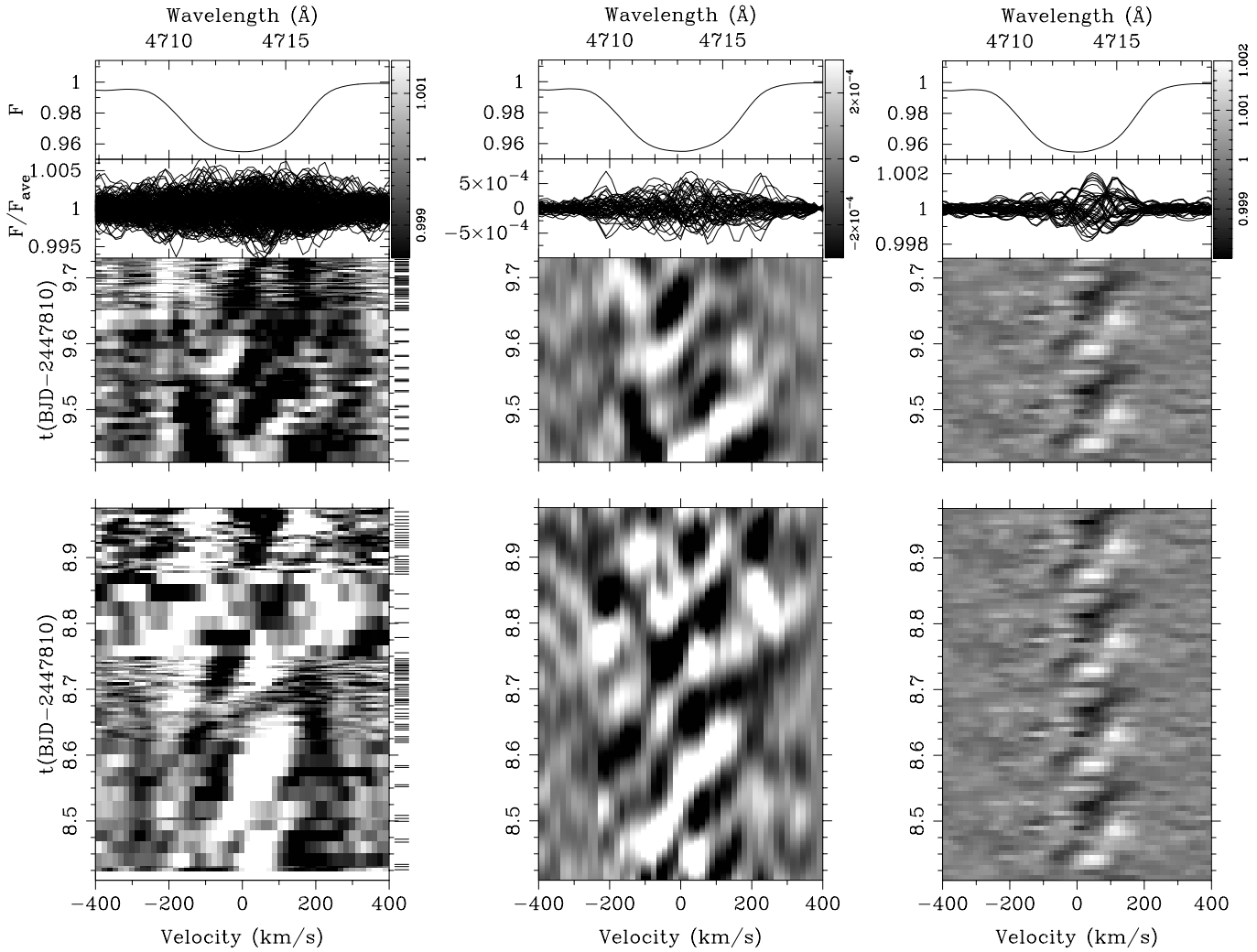

Fig. 2. Figure at the left: dynamic quotient spectra of 2 nights of ξ Per data. Horizontal lines indicate the mid-exposure times. The upper panel shows the average spectrum used to create the quotient spectra which are shown in the panel below. Note the slight depression at the left part of the average spectrum, caused by an unidentified line. Middle figure: inverse Fourier transform for which frequencies only above 2 c d^{-1} were used (see Sect. 3). Figure at the right: all data folded with a 3.5 h period, rebinned to 25 points per cycle

spite of our efforts to remove them. In the following we ignore this frequency range. In the uncontaminated areas (above 1.5 c d^{-1}) significant power is found across the line profile at several frequencies, visible as horizontal grey areas in the figures, which we attribute to NRP. The frequencies quoted in Sect. 4 were determined by first fitting in each velocity bin a Gaussian function to the peak in the power $\mathcal{P}(f)$:

$$\mathcal{P}(f) = \mathcal{P}_{\max} \exp(-(f - f_0)^2/2{\sigma_f}^2). \quad (1)$$

This yields three parameters: the maximum power $\mathcal{P}_{\max}$, the central frequency f_0 and the width of the peak σ_f. To determine the uncertainty ϵ_f in f_0 the height of the peak relative to the noise level, defined as N^2, should be taken into account. For this purpose we use the width of the peak at $\mathcal{P}_{\max} - N^2$, following Schwarzenberg-Czerny (1996). Applying Eq. 1 gives:

$$\epsilon_f = \sigma_f \sqrt{-2 \ln \left(1 - \frac{N^2}{\mathcal{P}_{\max}}\right)}. \quad (2)$$

We use a conservative method to calculate the noise level, which is a critical parameter: we defined N^2 as the power below which 95% of the datapoints fall in the histogram of the periodogram between 5 and 10 c d^{-1}. For ξ Per we find $N^2 = 2.4 \times 10^{-8}$ and for λ Cep $N^2 = 2.2 \times 10^{-8}$. We have chosen this procedure because white noise gives low and high peaks at all frequencies and apart from this it is not always clear whether a peak is only noise or contains a weak periodic signal.

Finally, the average frequency across the line profile was computed in two ways: a normal average with its standard deviation and an error-weighted average. In the latter method the uncertainty in the average is directly derived from the errors, ϵ_f, using the following equations:

$$\overline{f} = \frac{\sum_{i=1}^{N} f_i / {\epsilon_f}_i^2}{\sum_{i=1}^{N} {\epsilon_f}_i^2} \quad (3)$$

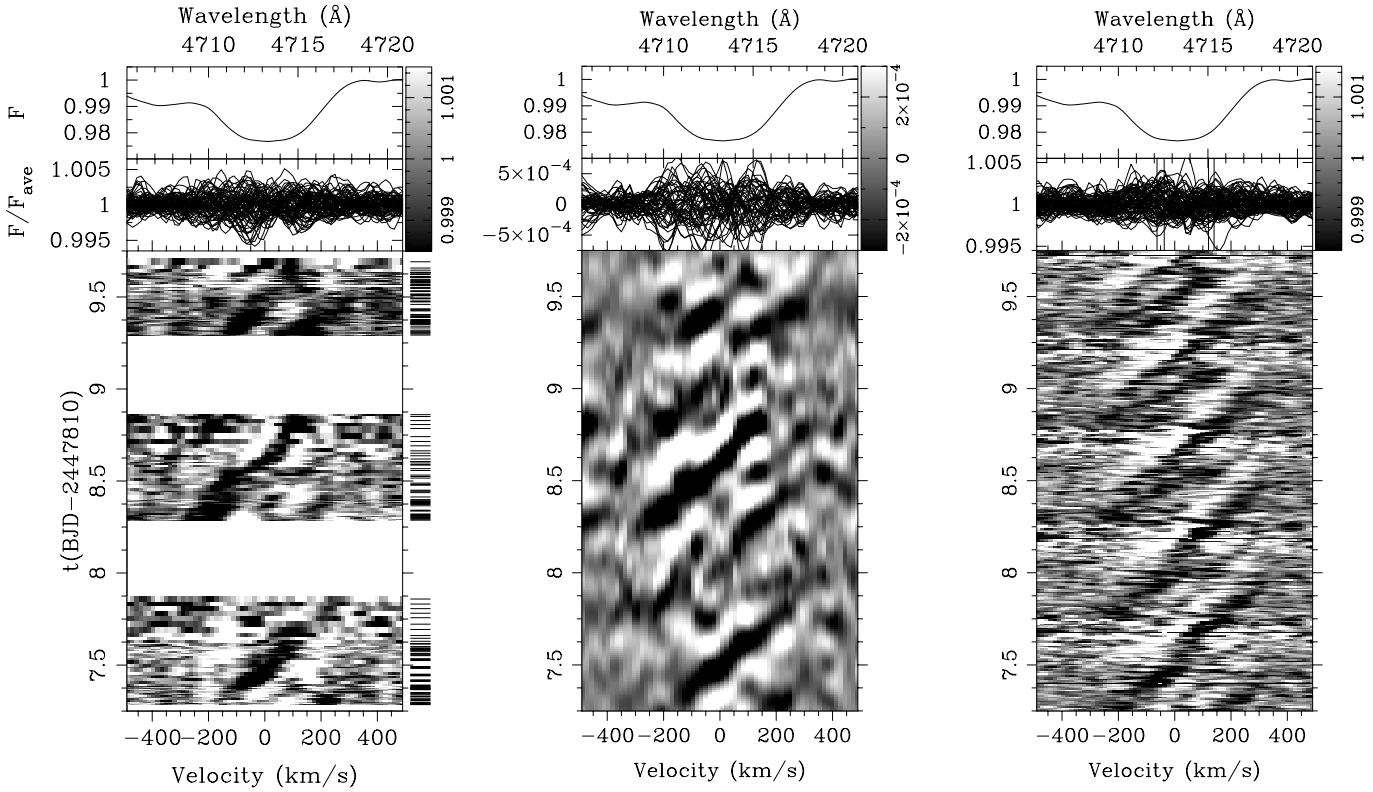

Fig. 3. Figure at the left: dynamic quotient spectra of 3 nights of λ Cep data, in similar format as in Fig 2. Middle figure: inverse Fourier transform using frequencies only between 1 c d^{-1} and 5 c d^{-1}. Figure at the right: sum of data folded by respectively 12.3 and 6.6 h and rebinned to timesteps of 0.0075

$$\overline{\epsilon_f}^2 = \frac{1}{\sum_{i=1}^{N} {\epsilon_f}_i^{-2}}. \quad (4)$$

In both cases we computed for every datapoint the deviation $d_i = |(f_i - \overline{f})/\sigma_f|$ where σ_f is the standard deviation. Secondly, we computed for each point the probability $P(d_i)$ of being a statistical fluctuation assuming a Gaussian distribution. We discarded all points for which $N \cdot P(d_i)$ is smaller than 0.5 (Chauvenet's criterion). In a sound statistical distribution both methods should give the same values. In case of differences we have chosen the method giving the largest error.

The phase of the signal can be extracted from the CLEANed Discrete Fourier Transform (CDFT), using the following representation:

$$F(t) = \Delta f \sum_{i=1}^{N} \sqrt{2\mathcal{P}_i} \cos(2\pi[f_i(t-\bar{t}) + \phi_i]). \quad (5)$$

Here $F(t)$ is the flux as a function of time, t, f_i is the frequency, Δf is the frequency interval $f_{i+1} - f_i$, $\mathcal{P}_i$ is the power, ϕ_i is the phase of component i, and $\bar{t}$ is the average time of the sample, used to relate the calculated phases to the Barycentric Julian Date (2447818.698 for ξ Per and 2447818.532 for λ Cep). By convention ϕ is defined between 0 and 1. Note that features with larger phase arrive earlier in time.

As an independent check we derived the phase information also from least-χ^2 multiple sine fits (components in Eq. 5) with frequencies fixed on the main peaks in the periodograms. We used 0.997, 9.138 and 7.956 c d^{-1} for ξ Per and 0.424, 1.96, 2.54 and 3.67 c d^{-1} for λ Cep. Error bars on the phases could then be derived by means of a Monte Carlo method in which artificial noise was added within the S/N limits of the data. In Figs. 5 and 7 we show the standard deviations σ_ϕ and $\sigma_{\rm A}$ of the phases and amplitudes resulting from 25 fits for each point. Before computing σ_ϕ the phases (ϕ_i) were anchored to the first calculated value using $\phi_i' = \phi_i - {\rm INT}(\phi_i - \phi_0 + 0.5)$. This assures that any value of ϕ_i' differs less than 0.5 from ϕ_0. The error bars are therefore not expected to exceed $\sqrt{1/12} \simeq 0.28$ which is the standard deviation of a uniform distribution with phases between 0 and 1 in absence of any signal. The apparently non-random distribution of the values of some phases outside the line profiles in Figs. 5 and 7 is unclear. We think that this might be caused by very small residual periodic variations in the continuum as seen in Figs. 2 and 3, rather than by a statistical dependency of the different points.

The quoted amplitudes and phases are determined from these multiple sine fits. These amplitudes are more reliable than from the CDFT's. This is because CLEAN removes the window-function effects component by component from the DFT, regardless whether the peak being removed contains some power of a real frequency. Consequently amplitudes in a CDFT may be smaller than they truly are. The phases determined by the two methods agree within the error bars.

As a comparison we reconstructed the pulsation patterns by inverting the DFTs and added all the components of Eq. 5 within the frequency range of interest, thereby filtering out a large fraction of the noise. We also folded the data with the detected periods. These two resulting reconstructions, in a grey-scale representation and appropriately rebinned, are shown in Figs. 2 and 3 along with the original data.

As an independent method for finding periods, complementary to the CLEAN analysis, we also performed a minimum-entropy method (Cincotta et al. 1995). In this method the time series are folded with trial periods, i.e. the phase of each observation is computed as $\phi = t/P - \mathrm{INT}(t/P)$. The phase/flux space is then divided into a number of grid elements in which the number of datapoints is counted. By defining the probability of finding a datapoint in element i as $p_i = N_i/N$ the entropy is calculated as $S = -\sum p_i \ln p_i$. The lower the value of S, the higher the probability that the trial folding period corresponds to a true period. The significance of the considered period follows from $\sigma^2 = (S - S_c)^2/\sigma_c^2$, where the index c refers to the continuum. In order to deal with the window function caused by the inhomogeneous data sampling, the minimum-entropy method was first performed after shuffling the data in a random manner, yielding S_0. Subtraction of S_0 from S removed in this way the periods caused by the window function.

4. Application and results

4.1. ξ Per (HD 24912)

In the periodogram (see Fig. 4) the most significant power outside the contaminated frequency range is found at f_1 = 6.96(4) c d^{-1} (or P_1 = 3.45(2) h) and at f_2 = 9.14(7) c d^{-1} (or P_2 = 2.63(2) h). The corresponding amplitudes and phases are displayed in Fig. 5. The phases for amplitudes less than 2σ above the continuum are not significant and are plotted as open symbols. We argue below why we do not consider f_2 as a significant period, and first consider f_1. Whereas the phase behavior of f_1 is clearly characteristic for a NRP, the asymmetry of the amplitude around line center is not, unless non-adiabatic temperature variations are important. In the profiles of ξ Per we find small equivalent-width (EW) changes, which could be in principle due to temperature effects. A CLEAN analysis of the EW variations show a few weak peaks in the power diagram, none of which correspond to any other known frequency in this star. The source of the EW variability is therefore probably noise. Temperature effects generate in general larger amplitudes in EW than we observe (although cancellations cannot be excluded), which makes us conclude that these effects are not likely to play a significant role (see Schrijvers & Telting 1998). Data with a higher S/N and better time resolution are needed to establish the (expected) first harmonic and to determine the azimuthal number m.

We investigated whether the relatively low power on the blue side at f_1 could be due to wind contamination. Simultaneously taken UV spectra (Kaper et al. 1999) show that a new DAC developed at low velocity around BJD 2447818.9. Similar simultaneous observations from another campaign on this star

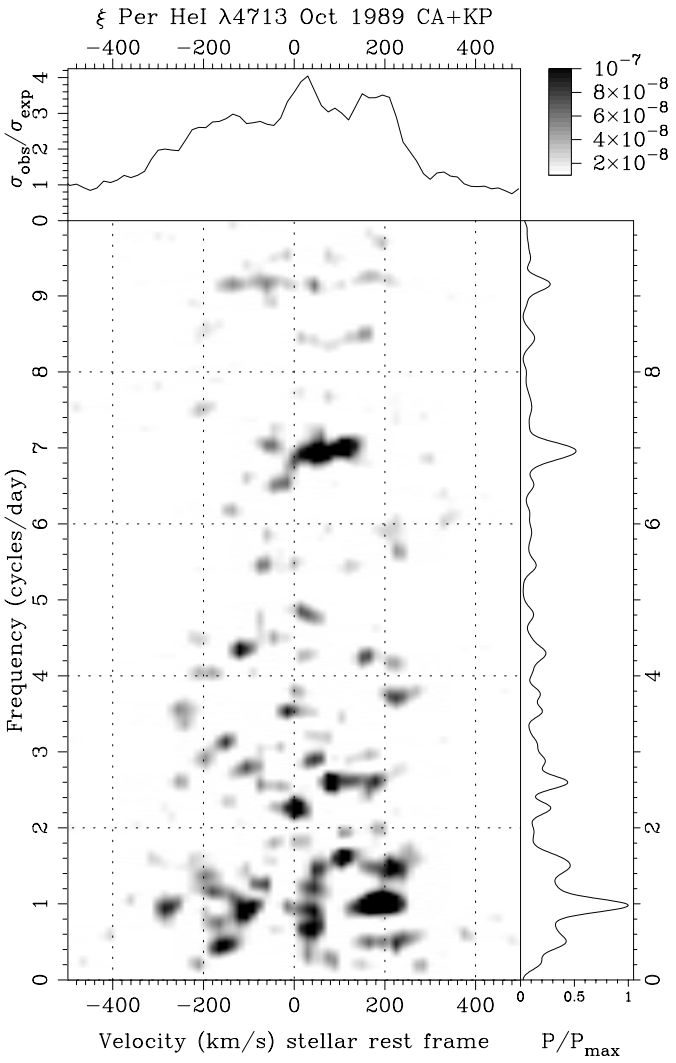

Fig. 4. Grayscale representation of the periodograms as a function of velocity of ξ Per spectra. The side panel shows the power summed over all velocities. The highest peak is normalized to unity. The top panel displays the ratio of the observed standard deviation to the expected standard deviation

(see Henrichs et al. 1998a) showed that the new development of a DAC is accompanied by enhanced blue-shifted absorption in Hα. The He I line presently studied is probably also partly formed in the wind and therefore should in principle display similar kind of extra absorption, which would disturb the period analysis. We therefore excluded the 24 spectra between BJD 2447818.975 and BJD 2447819.1 in our further period analysis. These spectra showed extra blue-shifted absorption which was not present in other spectra, and which we attribute to wind effects. This procedure indeed decreased somewhat the asymmetry in amplitude, although not completely. Some wind absorption is undoubtedly still present in a number of spectra, but a thorough elimination is beyond hope. A second cause might be a blending effect by the partly overlapping (unidentified) weak lines in the alleged blue continuum which may have distorted the normalization. We consider this as less important.

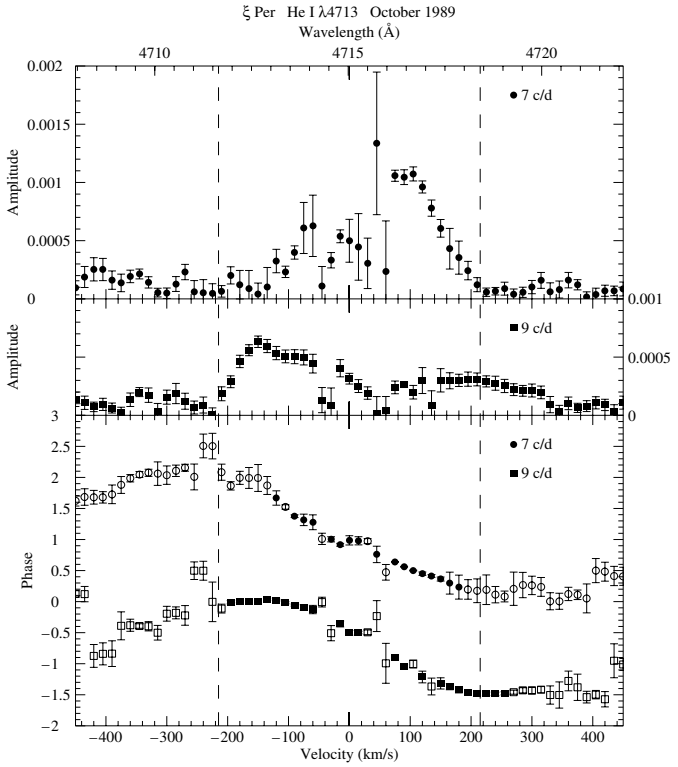

Fig. 5. Amplitude and phase (in 2π radians) of the signal at P_1 = 3.45 h (7 c d^{-1}) and P_2 = 2.63 h (9 c d^{-1}, not believed to be real). The vertical dashed lines are drawn at $\pm v\sin i$. The top scale is the observed wavelength

We furthermore folded the spectra with P_1 (right panel in Fig. 2). This shows a clear NRP pattern in the range from -100 to 160 km s^{-1}, less asymmetric around zero velocity than Figs. 4 and 5 suggest. Although the asymmetry in power remains worrisome, more evidence for P_1 being a true period in this star comes from observations of the O III λ5592 line taken during the MUSICOS November 1996 campaign (see Henrichs et al. 1998b), which also clearly show the NRP pattern over the whole line profile. This dataset was however insufficiently sampled to determine any NRP frequencies.

Considerable power is also found at f_2 = 9.14(7) c d^{-1} (or P_2 = 2.6(2) h) over almost the whole line profile (see Fig. 4). Several reasons argue against an interpretation in terms of NRP, however. First, the minimum-entropy analysis (see Sect. 3) did not reveal any signal around f_2, whereas f_1 was detected with 15σ significance. Secondly, the phase behaviour is suspiciously similar to that of f_1 (see Fig. 5). In addition, the amplitude increases where the amplitude of f_1 decreases, which may point towards interference. For these reasons we do not consider f_2 as a NRP frequency.

From the phase diagram belonging to f_1 we can derive the azimuthal degree, ℓ, according to Telting & Schrijvers (1997, hereafter TS) by measuring the difference in phase at ± 230 km s^{-1}, i.e. just outside $\pm v\sin i$ of the star. We note that our adopted $v\sin i$ value is in accordance with Penny (1996), although Howarth et al. (1997) find 213 km s^{-1}. From Fig. 5 we derive $\Delta\Psi(f_1) = 2\pi\times 1.6(2)$, where we had to use a linear extrapolation of a fit through the region between -125 and 180 km s^{-1} because outside these regions the phase is likely to be poorly defined due to the very low amplitudes.

Table 2 of TS lists coefficients of empirical linear fits to input and output ℓ values of synthetic data generated by Monte Carlo calculations for various pulsation parameters. We show below that in our case the ratio of horizontal to vertical motions, k, is small, certainly less than 0.3. This constraint gives for $\Delta\Psi(f_1)$ the result ℓ_1 = 3.4(5) with 88% confidence that the ℓ value is correct within ± 1. We adopt ℓ_1 = 3 as the most probable value for the harmonic degree. A higher or lower ℓ value would show up as one more or one less absorption feature in the line profile, which is not seen (Fig. 2). Since the first harmonic of this signal (at 14 c d^{-1} or 1.75 h) could not be detected in our dataset because the sampling rate was too low, we have no means to derive a value for the azimuthal parameter m.

We can determine the direction of the pulsation mode if the stellar rotation rate is known. Periodicities in stellar wind features suggest that the rotation period, $P_{\rm rot}$, is 2 or 4 days (Kaper et al. 1999). We obtain in both cases that the mode must be prograde. The value of k is in the (here justified) Cowling approximation related to the pulsation frequency, $f_{\rm co}$, in the corotating frame: $k = GM/R^3(2\pi f_{\rm co})^2$. Two rather differing values for the mass and radius are known: Leitherer (1988) finds 35 M$_\odot$ and 12 R$_\odot$ (case 1), not differing very much from earlier determinations, and also in agreement with the values given by Howarth & and Prinja (1989), whereas Puls et al. (1996) derive 60 M$_\odot$ and 25.5 R$_\odot$ (case 2) with new model-atmosphere fits, including wind effects. Even with the distance limits set by HIPPARCOS no preference can be given to either set. We can exclude a 4-day rotation period in case 1 because the implied rotation velocity would be lower than the observed $v\sin i$ value, whereas a 2-day period is excluded in case 2, since the star would rotate at break-up. In both remaining combinations (case 1 with $P_{\rm rot}$ = 2 d and case 2 with $P_{\rm rot}$ = 4 d) the inclination angle turns out to be close to 40°. The corresponding corotating frequencies, derived from $f_{\rm co} = f_{\rm obs} - |m|f_{\rm rot}$, are $f_{\rm 1co}$ = 5.4 c d^{-1} and $f_{\rm 2co}$ = 6.2 c d^{-1}, which give $k_1 \leq 0.05$ and $k_2 \leq 0.007$, because $|m| \leq \ell$. Such small values of k imply small horizontal atmospheric motions, characteristic of a p-mode.

4.2. λ Cep (HD 210839)

Outside the contaminated frequency range we find significant power at two different frequencies: at f_1 = 1.96(8) c d^{-1} (or P_1 = 12.3(5) h) and at about twice this frequency at f_2 = 3.64(14) c d^{-1} (or P_2 = 6.6(3) h), see Fig. 6. The minimum-entropy analysis yielded for these signals a significance of 10σ and 8σ, respectively. The corresponding amplitudes and phases are displayed in Fig. 7. The power of the first period appears to be concentrated mostly on the blue side of the line. This could be caused by interference of the unidentified line which is displaced by about -400 km s^{-1} with respect to the He I line, and which is stronger than in ξ Per. This secondary NRP pattern can clearly be seen in the folded spectra (Fig. 3). From the phase diagram

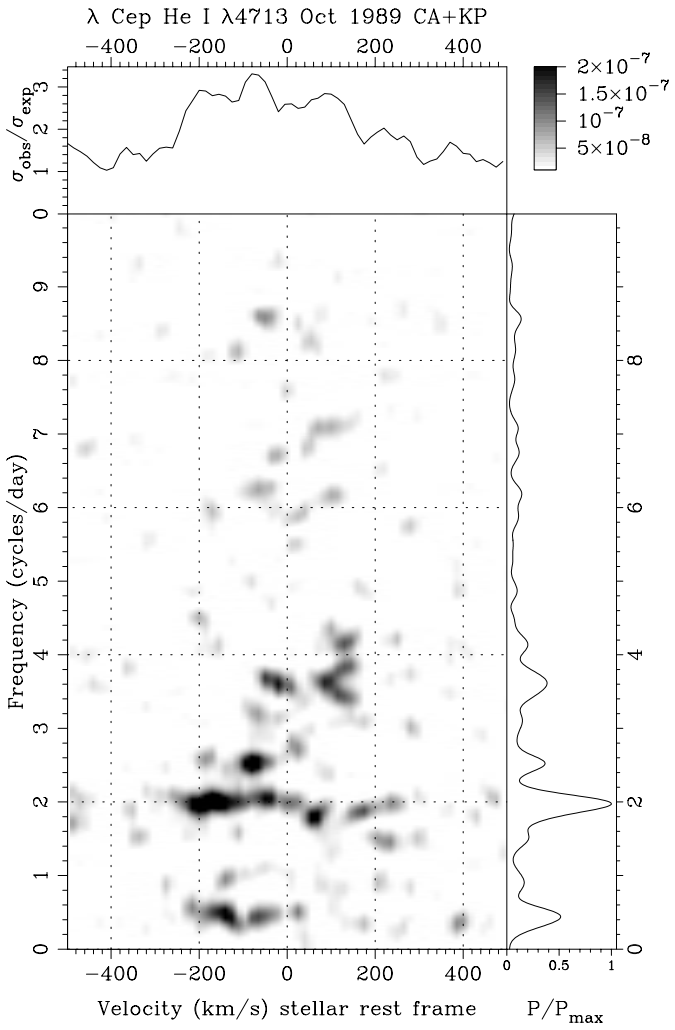

Fig. 6. Periodogram of λ Cep spectra. The layout is the same as in Fig. 4

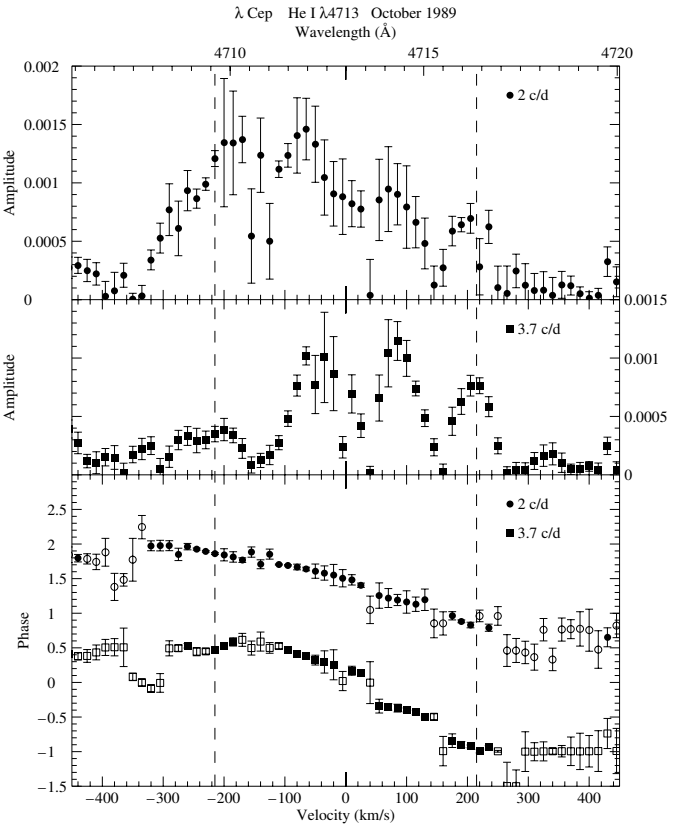

Fig. 7. Amplitude and phase (in 2π radians) of the signals at P_1 = 12.3 h and P_2 = 6.6 h. The layout is similar to Fig. 5

of the larger period we derive an ℓ value with the same method as above by measuring the difference in phase at $\pm 250\,\mathrm{km\,s^{-1}}$, again just outside $\pm v\sin i$ of the star. Our adopted $v\sin i$ value is in accordance with Penny (1996), not very different from $217\,\mathrm{km\,s^{-1}}$ given by Howarth et al. (1997). We find $\Delta\Psi(f_1) = 2\pi\times 1.3(1)$. The irregular phase jumps near $-160\,\mathrm{km\,s^{-1}}$ are likely caused by the very low power at these velocities, which are probably due to imperfectness of our dataset. We use here the $\ell - |m| < 2$ restricted fit, which gives $\ell_1 = 2.9(3)$ according to TS. We adopt therefore $\ell_1 = 3$ as the most probable value.

Although f_2 is nearly twice f_1, it cannot be its first harmonic since the ratio $f_2/f_1 = 1.86(10)$ deviates more than 1σ from the exact value of 2. In addition, in all velocity bins the power at f_2 lies systematically below the power at $2f_1$ (see Fig. 6). This makes the probability of f_2 being a harmonic of f_1 less than 10^{-5}. We could also exclude f_2 being a harmonic by considering the consistency check for the amplitude ratio and the phase relation of the main frequency and its first harmonic as given by TS. They find that $\Psi_{12} = 2\Psi_1 - \Psi_2 = \pi\times 1.50(6)$, where the phase at line center of the main frequency is denoted by Ψ_1 and of the first harmonic by Ψ_2. For λ Cep we obtain $\Psi_{12} = \pi\times 1.6(3)$. This would give fair confidence that the higher frequency could indeed be the first harmonic of the lower, except that in all model calculations by TS the ratio of the amplitudes of the first harmonic to the main frequency is considerably smaller than we observe, which makes f_2 as a first harmonic very unlikely, which we therefore consider as a second NRP mode.

For the second mode we find $\Delta\Psi(f_2) = 2\pi\times 2.4(3)$. From this value we derive $\ell_2 = 5.2(7)$ using a $k < 0.3$ fit with 86% confidence, which implies $\ell = 5$ as the most probable value for this second NRP mode and m remains undetermined. This mode complies with the number of bumps seen at any given time in the folded spectra in Fig. 3.

Adopting an upper limit to the rotation period of 4.5 days, using a radius of 19 $R_\odot$, a mass of 59 $M_\odot$ (Puls et al. 1996) and an inclination angle of 90°, we find that the corotating frequencies are 1.29 c d^{-1} for the $\ell = 3$ mode, implying $k < 0.38$, and 2.53 c d^{-1} for the $\ell = 5$ mode, corresponding to $k < 0.1$. Both modes are therefore prograde modes, and could be a p or g mode, depending on the adopted stellar model.

5. Model calculations

From the observed amplitudes in the line profiles one can derive the velocity amplitude of the pulsation. To obtain a crude estimate we considered for simplicity a single sectoral p-mode

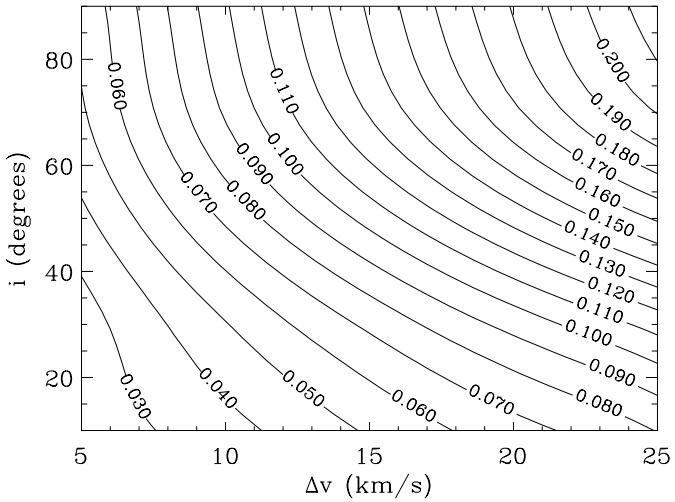

Fig. 8. Contour plot of calculated relative amplitudes of the He I λ4713 line profile as a function of the pulsation velocity semi-amplitude Δv and inclination angle i. The curves are based on 25 model calculations with stellar atmosphere parameters corresponding to ξ Per with $\log g$ = 3.4 and $T_{\rm eff}$ = 36 000 K (Puls et al. 1996)

($\ell = |m|$), i.e. without horizontal velocity component (k = 0), and no temperature variations. We divided the visible stellar surface in about 2500 elements. The grid is further defined by the inclination angle, i, rotational velocity, $v_{\rm rot}$, and pulsation velocity semi-amplitude Δv. For each grid element we calculated specific intensities and limb darkening of the He I λ4713 line for the given stellar parameters ($T_{\rm eff}$ and $\log g$) using atmosphere models created by TLUSTY and SYNSPEC by Hubeny & Lanz (1992). For each grid element the radial velocity and angle towards the observer is computed. Using these values, Doppler-shifted specific intensities as function of v are interpolated from the model atmosphere. Finally, the line profile was calculated by integrating the intrinsic line profiles of all grid elements over the visible surface. For a given inclination angle and pulsation amplitude 20 profiles were calculated spread over a full period and the profile with the largest amplitude at line center was selected. At that particular phase the inclination and Δv were varied in the domain of Fig. 8 and the maximum amplitude was measured. We applied this method to ξ Per using $T_{\rm eff}$ = 36 000 K and $\log g$ = 3.4 (Puls et al. 1996, case 2 in the above). We computed 25 models in the $\Delta v - i$ plane between 5 and 25 km s^{-1} and from 10 to 90° respectively. The resulting semiamplitudes relative to the line depth, $A_{\rm rel}$, are shown as contours in Fig. 8.

In ξ Per the central depth of the He I line is 4% and the amplitude only 0.12% of the local continuum (see Fig. 5), which means that the NRP signal is weak with $A_{\rm rel}$ = 0.03. Following the corresponding contour in Fig. 8 we derive that Δv can be at most about 5 km s^{-1} for the adopted $i \sim 40°$.

For λ Cep the stellar parameters are not too different from those of ξ Per (although k is larger), and we simply applied the same calculations for this star as a first approximation. The central depth of the line is 2% and the amplitude 0.11%, implying $A_{\rm rel}$ = 0.06. For an inclination angle of $i \sim 90°$ this gives $\Delta v \sim 6$ km s^{-1} for this star. The inclination cannot be much lower according to the stellar parameters (see Sect. 4.2). From a sample calculation we found that a model atmosphere for λ Cep has nearly the same limb darkening and width of the intrinsic profiles as for ξ Per, which are the main quantities on which the NRP amplitude depends. In spite of all these approximations we consider the derived value for λ Cep to be quantitatively justified.

6. Discussion

The length and coverage of our datasets, combined with known cyclical wind effects limit the frequency range in which we can detect pulsation periods from about 1.5 to 10 c d^{-1}. Of course we cannot rule out the presence of other modes in these stars. In fact it is likely that more modes will be found with better datasets like for example in the case of the O9.5V star ζ Oph (Kambe et al. 1993, Reid et al. 1993, Kambe et al. 1997, Jankov et al. 1998) where increasingly higher-quality spectra and denser coverage revealed a larger number of modes, up to ℓ = 18.

The presence of NRP in ξ Per was already suspected by Gies & Bolton (1986) on the basis of radial velocity variations, which they assumed to be due to NRP, but no significant period or mode could be identified from their sample of 38 photographic spectra. Significant profile variability in many lines (except in λ4713 Å!) was also found by Fullerton (1990), but no mode or period could be established.

A preliminary analysis of the data of the present paper on λ Cep was given by Henrichs (1991), who found the ℓ = 5 NRP mode with a 6.5 h period, and mentioned the possible presence of the ℓ = 3 mode at 12.5 h. Walker (1991) reported a likely ℓ = 5 or 6 mode (no period) for this star, but without further details we cannot compare his results with ours.

We also find small EW variations in this star, and some frequencies do coincide approximately with the pulsation frequencies. They could in principle be to be due to temperature effects. Higher-quality data are needed to confirm this.

Marchenko et al. (1998) report the presence of a strong 0.63 day period in the HIPPARCOS photometry of λ Cep (but none in ξ Per) over the 3.5 year lifetime of the satellite, which partly covered our campaign. This period is not compatible with any of the NRP or wind periods, and its origin is unclear.

We now return to the question set out at the beginning of this research whether non-radial pulsation can be the origin of the cyclical wind variability. If the mode we found is the only mode in ξ Per, it appears that the pattern speed of the waves running around the star superposed on the rotation (see Sect. 3.1) is too high to be compatible with the observed wind periods (1, 2, 4 days). This is probably true for most short-period single mode pulsations, since for most O stars the rotation rate is much lower. An exception is the O4 star ζ Pup, for which Reid and Howarth (1996) report evidence for a direct connection between wind features and an NRP mode. They found both in Hα up to $0.3v_\infty$ and in He II λ5411 the same period of 8.54h. However, they consider the 19.6h period found in IUE observations incompatible with this NRP period.

The presence of multimodes, however, has possibly interesting consequences for the origin of cyclical wind variability (see also Rivinius et al. (1998) for the Be star μ Cen). Consider for example a case with two different prograde sectoral modes, traveling around the star with different frequencies. A given crest of the faster wave will at a certain moment overtake a crest of the slower wave, which means an enhancement of the total amplitude at a certain longitude. The next enhancement will be when a different crest will overtake, but this will be at a different longitude. This will give rise to cyclical surface amplitude enhancements which may cause wind perturbations that are related to the relative traveling speeds and the m values of the NRP waves. The simultaneous presence of more than two modes will increase the complexity of this beating effect. Observations show, however, that the periods of cyclical wind variability of O (and B) stars scale with the rotation period of the stars (Prinja 1988, Henrichs et al. 1988), and it is difficult to understand how this could be related to the above described effect of beating NRP modes.

We therefore think that the best candidate for the cause of the cyclical wind variability still remains the presence of weak magnetic fields on the surface, corotating with the star. A proof has to wait for a systematic deep survey of these fields. A preliminary upper limit of 70 G on the longitudinal component of the magnetic field strength of ξ Per was presented by Henrichs et al. (1998a).

In conclusion, if our interpretation is correct, the number of confirmed O stars with NRP is now about 6 (see Fullerton et al. 1996, including ζ Pup). In the light of asteroseimological applications, we note that 5 of these are runaways. Although the statistics are limited, OB runaway stars tend to rotate rapidly and to have an enhanced surface He abundance (Blaauw 1993). These factors might play a role in exciting the NRP. The exception is the pulsator 10 Lac, which is not classified as a runaway star, but this star is associated with a bow shock detected on IRAS 60 micron maps (van Buren et al. 1995), indicating a post binary mass-transfer history, and hence a different internal structure is likely, perhaps favouring the existence of NRP modes.

Because of the known ubiquity of line-profile variables among O stars it one can expect that with a concentrated observational effort with sufficient S/N, coverage and time resolution, more pulsation-mode identifications in O stars are likely to follow. Higher spectral resolution is needed to find possible multimodes in these stars. The possible consequence of such multimodes for cyclical wind behavior needs to be investigated.

Acknowledgements. The help of skillful staffs at the Calar Alto and Kitt Peak observatories is highly appreciated. HFH thanks Rolf Kudritzki and his colleagues for their warm hospitality and encouragement during the period that this work was initiated, and for his suggestion to concentrate on the He I λ4713 line for searching for pulsations. We thank Mariano Méndez for drawing our attention to the minimum-entropy analysis and help. We are also grateful to the referee Alex Fullerton for his constructive comments. JAdJ acknowledges support by the Netherlands Foundation for Research in Astronomy (NFRA) with financial aid from the Netherlands Organization for Scientific Research (NWO) under project 781-71-053.

References

Blaauw A., 1993, In: Cassinelli J.P., Churchwell E.B. (eds.) Massive stars: their lives in the interstellar medium. ASP Conf. Ser. 35, p. 207
Cincotta P.M., Méndez M., Nunez J.A., 1995, ApJ 449, 231
Conti P.S., Ebbets D., 1977, ApJ 213, 438
Cranmer S.R., Owocki S.P., 1996, ApJ 462, 469
Fullerton A.W., 1990, Thesis, University of Toronto
Fullerton A.W., Gies D.R., Bolton C.T., 1996, ApJS 103, 475
Gies D.R., 1987, ApJS 64, 545
Gies D.R., Kullavanijaya A., 1988, ApJ 326, 813
Gies D.R., Bolton C.T., 1986, ApJS 61, 419
Henrichs H.F. 1991, In: Baade D. (ed.) ESO Workshop on Rapid variability of OB stars: Nature and diagnostic value. p. 199
Henrichs H.F., Kaper L., Zwarthoed G.A.A., 1988, In: A Decade of UV Astronomy with the IUE Satellite (ESA SP-281), Vol.2, p. 145
Henrichs H.F., de Jong J.A., Kaper L., Nichols J.S., et al., 1998a, UV Astrophysics Beyond the IUE Final Archive, ESA-SP 413, p. 157
Henrichs H.F., de Jong J.A., Catala J.-F., et al., 1998b, Proc. Cyclical variability in stellar winds, ESO workshop October 1997, p. 374
Henrichs H.F., Kaper L., Nichols J.S., 1994, A&A 285, 565
Howarth I.D., Prinja R., 1989, ApJS 69, 527
Howarth I.D., Siebert K.W., Hussain G.A.J., et al., 1997, MNRAS 284, 265
Howarth I.D., Townsend R.H.D., Clayton M.J., et al., 1998, MNRAS 296, 949
Hubeny I., Lanz T., 1992, A&A 282, 157
Jankov S., Janot-Pacheco E., Leister N.V., 1998, preprint
Kambe E., Ando H., Hirata R., 1993, A&A 273, 450
Kambe E., Hirata R., Ando H., et al., 1997, ApJ 481, 406
Kaper L., Henrichs H.F., Nichols J.S., et al., 1996, A&AS 116, 1 (paper I)
Kaper L., Henrichs H.F., Nichols J.S.,et al.,1999, A&A, in press (paper II)
Kiriakidis M., Fricke K.J, Glatzel W., 1993, MNRAS 264, 50
Leitherer C., 1988, ApJ 326, 356
Marchenko S.V., Moffat A.F.J., van der Hucht K.A., et al., 1998, A&A 331, 1022
Mullan D.J., 1984, ApJ 283, 303
Penny L.R., 1996, ApJ 436, 737
Prinja R.K., 1988, MNRAS 231, 21P
Puls J., Kudritzki R.-P., Herrero A.,et al., 1996, A&A 305, 171
Reid A.H.N., Bolton C.T., Crowe R.A., et al., 1993, ApJ 417, 320
Reid A.H.N, Howarth I.D., 1996, A&A 311, 616
Rivinius Th., Baade D., Stefl S., et al., 1998, A&A 336, 177
Roberts D.H., Lehar J., Dreher J.W., 1987, AJ 93, 968
Schrijvers C., Telting J.H., 1998, A&A, in press
Schwarzenberg-Czerny A., 1996, ApJ 460, 107
Telting J.H., Schrijvers C., 1997, A&A 317, 723
Van Buren D., Noriega-Crespo A., Dgani R., 1995, AJ 110, 2914
Walker G.A.H. 1991, In: Baade D. (ed.) ESO Workshop on Rapid variability of OB stars: Nature and diagnostic value. p. 27